

Electrolyte Role in SEI Evolution at Si in the Prelithiation Stage vs the Post-lithiation Stage

To cite this article: Saida Cora et al 2023 J. Electrochem. Soc. 170 020507

View the article online for updates and enhancements.

You may also like

- Recent Progress in Cu Electrodeposition for TSV (Through Silicon Via) Jae Jeong Kim, Myung Jun Kim, Seunghoe Choe et al.
- Study on the dislocation mechanism of Ni₄₇Co₅₃ alloy during rapid solidification Yun-chun Liu, Yong-chao Liang, Qian Chen et al.
- Mathematical Modeling of Inhibitor Transport in an Organic Coating Kerry Allahar, Michael Hurley, Erik Sapper et al.





Electrolyte Role in SEI Evolution at Si in the Pre-lithiation Stage vs the Post-lithiation Stage

Saida Cora,**,1 Daris Key, John Vaughey,2,* and Niya Sa1,z D

¹Department of Chemistry, University of Massachusetts Boston, Boston, Massachusetts, 02125, United States of America ²Chemical Sciences and Engineering Division, Argonne National Laboratory, Lemont, Illinois, 60439, United States of America

The formation and evolution of the dynamic solid electrolyte interphase (SEI) at the Si anode/electrolyte interface are yet to be completely understood to solve irreversible capacity loss and increase battery cycle life. Herein, the evolution of SEI and its dynamic properties at the Si anode/electrolyte interface are investigated in two electrolyte systems, a 1.2 M LiPF₆ in EC: EMC 3:7 (wt%) electrolyte (referred to as Gen2) and a 1.2 M LiTFSI in EC: EMC 3:7 (wt%) electrolyte (referred to as LiTFSI). Two lithiation stages are studied: the pre-lithiation (pre-Li) SEI stage and the post-lithiation (post-Li) stage. Findings reveal at the pre-Li, SEI formation starts at an early potential and contributes to the greater mass gain in the Si/Gen2, and it is dominated by the formation of a non-uniform F- and P-rich layer in Si/Gen2, in contrast to a homogeneous F- and C-containing layer at the Si/LiTFSI interphase. The initially formed SEI in LiTFSI further benefits the charge transfer kinetics. At the post-Li stage, a more substantial SEI evolution is observed at Si/LiTFSI. This study offers a foundational understanding of the SEI dynamic evolution with electrolyte dependence. Findings from this report offer important insights into solving the complex SEI stability issues on Si. © 2023 The Electrochemical Society ("ECS"). Published on behalf of ECS by IOP Publishing Limited. [DOI: 10.1149/1945-7111/acb617]

Manuscript submitted December 7, 2022; revised manuscript received January 13, 2023. Published February 7, 2023.

Supplementary material for this article is available online

Rechargeable batteries sparked a revolution in the energy industry and rapidly grew in popularity in the past few decades with lithium-ion batteries (LIBs) becoming the current state-of-theart technology. The demand for the enhanced performance of electric vehicles created a strong need to design beyond LIB alternatives with higher energy densities and low cost. The shift from traditional intercalation-type anodes to alloying-type chemistries is one promising strategy to improve the energy density of beyond LIBs. 1-3 Alloy-type Si anodes have been intensively studied as one of the most promising anode materials to potentially replace conventional graphite in LIBs owing to its low cost and high gravimetric capacity (3579 mAh g⁻¹ for Si and 372 mAh g⁻¹ for graphite). However, the practical application of Si anodes is limited by the formation of an unstable solid electrolyte interphase (SEI) caused by large volume variations (~300%, Li₁₅Si₄) and cracking of the Si material during alloying/dealloying, promoting continuous SEI evolution.^{7–10} Unstable SEI results in low cycling efficiencies and severe capacity fade due to side reactions at the Si surface and continuous consumption of active electrolyte components. Several strategies have been reported to improve the SEI stability on Si. Commonly proposed methods include nanostructuring, chemical modification, and growth of the sacrificial surface layers. 11-14 However, these approaches induce higher costs with low yields and limited commercial practicality.

One of the most attainable and cost-effective strategies to stabilize the SEI on Si is to employ electrolyte systems that dominate the SEI growth. The choice of electrolyte has been reported to play a crucial role in the interfacial reactivity of Si anode and the evolution of the electrolyte-dependent SEI.¹⁵ The widely used lithium hexafluorophosphate (LiPF₆)-based electrolytes, such as Gen2 (1.2 M LiPF₆ in ethylene carbonate (EC) and ethyl methyl carbonate (EMC) 3:7 by wt%), are preferred in industry and academic fields due to their high solubility in carbonate solvents and cost-effectiveness. However, LiPF₆ is known to have a number of issues that negatively impact its electrochemical performance, for instance, its high sensitivity to moisture and low thermal stability (up to 70° C). Hold The decomposition of PF₆ anion was reported to yield LiF and PF_v as the major SEI components on the Si surface while the

reactivity of PF₆⁻ anion to trace water to form HF may lead to corrosion of materials. ^{20,21} The recently popularized imide-based salt, lithium bis(trifluoromethane sulfonyl)imide (LiTFSI), is suggested to be a promising alternative to the widely used LiPF₆ counterpart owing to its low sensitivity to hydrolysis, higher ionic conductivity than LiPF₆, and excellent anodic stability. ^{22,23} However, little is known about SEI development and its evolution upon electrochemical cycling at these interfaces, but these are the key properties influencing reversible capacity and cycle life. Although several *ex* situ studies have investigated the SEI morphology and composition on Si, they were mostly limited by surface characterizations such as Furrier transform infrared spectroscopy (FTIR), X-ray photoelectron spectroscopy (XPS), atomic force microscopy (AFM), and scanning electron microscopy (SEM) which compromise the electrochemical consequence and mechanical integrity of SEI. ^{24–28}

In this study, we investigate the in situ evolution of the Si/Gen2 and Si/LiTFSI interfaces with real-time monitoring of gravimetric, electrochemical, and physical changes by employing electrochemical quartz crystal microbalance coupled with in situ dissipation monitoring (EQCM-D). Two lithiation stages are investigated: prelithiation (pre-Li) SEI formation from open circuit voltage (OCV) to 0.5 V, and post-lithiation (post-Li) stage from 0.5 V to 0.001 V. Findings show that SEI growth and evolution are dynamic processes. The mass gain/loss at the interface is quantified by EQCM-D and the electronic nature of SEI is probed by electrochemical impedance spectroscopy (EIS). Results reveal that the SEI evolution is notably different in Si/Gen2 and Si/LiTFSI at pre-Li vs post-Li stages. At the pre-Li stage, an earlier and gravimetrically greater SEI is formed in Gen2 electrolyte vs LiTFSI, with inhomogeneous surface morphology consisting of a fragmentary F- and P-rich SEI. In contrast, at the post-Li stage, continuous SEI evolution is seen in Gen2 while a more substantial contribution to the SEI development is observed in LiTFSI at lower lithiation potentials, with the formation of a F-, C- and S-rich SEI. The earlier-formed fluorinated SEI in Si/Gen2 enhanced the charge transfer kinetics while in Si/ LiTFSI, an initial non-conductive SEI is formed and later converted to having facile charge transfer kinetics in the *post-Li* stage where more significant decomposition of the TFSI anion takes places. To the best of our knowledge, the findings in this work present the first report distinguishing the pre-Li and post-Li stages of electrolyte-dependent SEI evolution at the Si/Gen2 and Si/ LiTFSI interfaces.

^{*}Electrochemical Society Member.

^{**}Electrochemical Society Student Member.

^zE-mail: saniyabnu@gmail.com

Experimental

Electrode and electrolyte preparation.—Si thin film electrodes were fabricated by using the DC magnetron sputtering (AJA International) method off an elemental Si target (99.999%, Kurt J. Lesker, USA) onto 5 MHz AT-cut quartz crystal resonators (Q-Sense, Biolin Scientific, Sweden). A thin layer of Cu was predeposited onto the quartz resonator from the elemental Cu target (99.999%, Kurt J. Lesker, USA) at 225 W magnetron power at the rate of 11.97 nm min⁻¹ for 60 s resulting in the layer thickness of ~12 nm. Amorphous Si thin films with ~60 nm thickness were obtained at 227 W in magnetron power for about 14 min at a rate of 4.129 nm/min. The base and working pressure of the chamber were 2.6×10^{-7} Torr and 3 mTorr, respectively. After deposition, samples were immediately transferred to an argon-filled glove box (Vacuum Technology Inc., H₂O and O₂ below 0.1 ppm) to minimize their exposure to air. The Gen2 electrolyte (1.2 M LiPF₆ in 3:7 by weight ethylene carbonate (EC) and ethyl methyl carbonate (EMC)) and 1.2 M LiTFSI in 3:7 by weight EC: EMC 3:7 were used as received (Tomiyama High Purity Chemical Industries Ltd, Japan).

EQCM-D and electrochemistry measurements.—Electrochemical quartz crystal microbalance measurements were carried out with a Osense instrument (Biolin Scientific, Sweden) located in the argon-filled glovebox (Vacuum Technology Inc.) with H₂O and O₂ under 0.1 ppm. The measurements were conducted using an in-house design electrochemical cell combined with an EQCM-D module. The EQCM-D resonators used in this work were AT-cut crystals with an area of 0.785 cm² and a fundamental resonance frequency of 5 MHz. The Si thin film coated EOCM-D resonator was used as a working electrode (WE) with lithium metal (99.9%, Goodfellow) as both the reference (RE) and counter (CE) electrodes. After the electrolyte was introduced into the EQCM-D cell, the baseline frequency and dissipation were recorded before the start of cyclic voltammetry (CV) measurements. The potential was applied at 1 mV/s from open circuit voltage (OCV) to 0.001 V (vs Li/Li⁺) and controlled by the Potentiostat (Princeton Applied Instruments). EQCM-D measurements were recorded at odd overtones (n = 3, 5, 7) using QSoft401 software. Data acquisition for the electrochemical measurements was performed using Versa studio.

FESEM and EDS characterization.—The morphologies and elemental mapping of the Si surface were characterized by a field

emission scanning electron microscope (FESEM, ZEISS Sigma 500, Germany) equipped with an energy-dispersive X-ray detector (EDS, Oxford Instruments, UK). Si thin film was discharged in a 2-electrode Swagelok cell with Gen2 or LiTFSI electrolytes and held at 0.5 V or 0.001 V vs Li⁺/Li for 1 hr. SEM micrographs of Si were collected at 2–3 kV accelerating voltage. The EDS elemental mappings were collected at 8 kV with the data analysis performed by the AZtec software package (Oxford Instruments, UK).

EIS measurement and fitting.—Electrochemical impedance spectroscopy (EIS) was measured in a 2-electrode Swagelok cell with Si thin film as WE and Li metal as RE and CE. The frequency range was set from 0.05 Hz to 1 MHz with an AC voltage amplitude of 10 mV. The cell was first cycled in Gen2 or LiTFSI electrolytes for five consecutive CVs with subsequent EIS collected at 1.2 V, 0.5 V, 0.005 V and 0.001 V. The EIS experimental data were fitted to the equivalent Randles circuit model using the AfterMath software (Pine Research Instrumentation, Durham, NC).

FTIR analysis.—Surface characterization of the cycled electrodes was performed ex situ using Nicolet iS50 Fourier transform infrared absorption spectrometer (FTIR) equipped with attenuated total reflectance (ATR) detector. FTIR spectra were collected by performing 64 scans with a spectral resolution of 8 cm⁻¹ in the range between 4000–400 cm⁻¹. The Si thin film serving as the working electrode was discharged in a 2-electrode Swagelok cell with Gen2 or LiTFSI electrolytes and held at 0.5 V or 0.001 V vs Li⁺/Li for 1 hr before the FTIR analysis. The cycled electrodes were rinsed with DMC and dried in the vacuum chamber, transferred through an inert atmosphere, and then mounted directly on the ATR stage and tightly clamped. The spectral measurements were performed outside the glovebox. Data collection and spectral calculations were performed using OMNIC software.

Results and Discussion

Electrolyte-dependent pre-lithiation SEI of Si at the first electrochemical cycle.—Electrolyte-dependent in situ SEI formation was investigated at two system interfaces, Si/Gen2 and Si/LiTFSI. The electrochemical reduction pathway is first explored in an inhouse designed EQCM-D cell, where the working electrode was a quartz resonator sputtered with a 60 nm Si thin film and Li metal

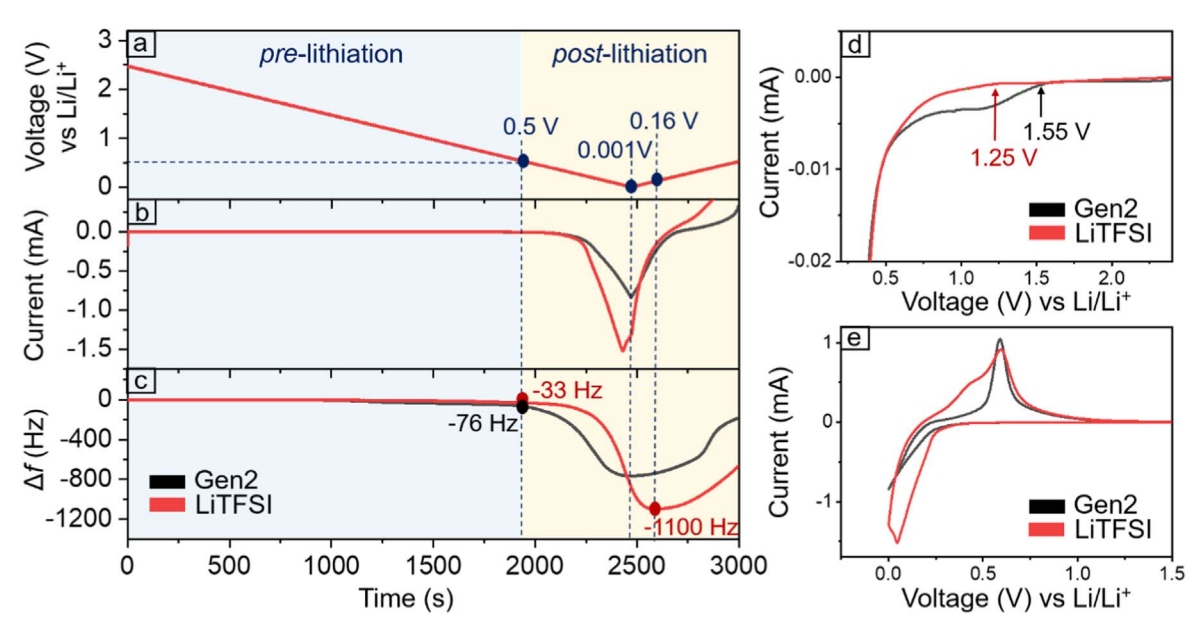


Figure 1. (a)–(c) Voltage, current and frequency (n = 3) changes over time for the first CV cycle from OCV to 0.001 V at 1 mV/s for Gen2 (black curve) and LiTFSI (red curve); (d) Electrolyte reduction pathway from OCV to 0.4 V for Gen2 (black curve) and LiTFSI (red curve); (e) Cyclic voltammograms of the first electrochemical cycle from OCV to 0.001 V vs Li/Li⁺ for Gen2 and LiTFSI electrolytes.

serving as counter and reference electrode. The electrolyte reduction contributed mass exchange at Si interface was characterized by the in situ EQCM-D with measured frequency shifts Δf (3rd overtone), and dissipation ΔD (3rd overtone). In this experiment, the cell voltage and current were simultaneously collected during the first electrochemical cycle along with the Δf and ΔD measurements. The estimated SEI thickness based upon Δf following the Sauerbrey correlation is presented in the Supporting Information.

Pre-Li SEI formation is defined at the potential from OCV (~2.5 V) to 0.5 V as presented in Fig. 1. Electrochemical decomposition of Gen2 is initiated at an earlier potential than LiTFSI electrolyte, for instance, the starting point of the electrolyte reduction voltage is at 1.55 V for Gen2 vs 1.25 V for LiTFSI, shown in Fig. 1d. The reductive current observed at voltages between 1.55 and 1.0 V for Gen2 (black) mostly originates from the reduction of the EC solvent, resulting in the formation of the carbonates such as ROCO₂Li, ROLi, or possible decomposition of the uncoordinated PF₆ anions that electrochemically react with the trace water in electrolyte to form LiF. 11,29–33 In contrast, reduction peaks for the LiTFSI electrolyte are not observed until the voltage sweeps down to 1.25 V, indicating the reduction of solvent molecules. In accordance with the literature, the decomposition of TFSI⁻ anion is not expected until lower potentials ($<1.0\,\text{V}$) to form several insoluble species at the interface, such as LiF, Li₂S and Li₂O.^{34–3}

Herein, a more detailed EQCM-D analysis is presented for three different voltage ranges at the pre-Li stage. From OCV (\sim 2.5 V) to 1.2 V, results suggest a greater mass change at Si/Gen2 interface vs Si/LiTFSI, and negligible surface adsorption is observed with no significant frequency drifts for both Gen2 and LiTFSI at OCV (Figs. 1a-1c). To confirm that the frequency shift is mainly contributed by the SEI formation rather than the surface adsorption of electrolyte, a control experiment of soaking Si thin film prior to the voltage sweep is performed. Results suggest contribution from electrolyte adsorption is negligible (detailed data and discussion can be found in SI, and Fig. S1). At a reducing potential of 1.2 V, a reductive current of $-3.2 \mu A$ is seen along with a 24 Hz frequency shift for Gen2, while a $-0.77 \mu A$ reductive current is seen along with a 7 Hz frequency change for LiTFSI (Fig. S2). The larger frequency decrease in Gen2 signifies the formation of a surface layer possibly as a consequence of a reductive decomposition of PF₆ anions along with EC reduction reported in the literature at $\sim 2.0 \text{ V}$ and $\sim 1.4 \text{ V}$ respectively. Furthermore, for reduction potentials from 1.2 V to 0.7 V, a decreased Δf simultaneous with higher reductive current are observed for both electrolytes suggesting further SEI growth. At 0.7 V, a 46 Hz Δ f along with a -4.7μ A current decrease are seen for Gen2 as compared with a 21 Hz Δf and a $-3.5 \mu A$ current decrease for LiTFSI (Fig. S2). At 0.5 V, a more significant frequency shift of 76 Hz is observed for Gen2 while a mere 33 Hz frequency shift is seen for LiTFSI with comparable currents at $-8.4 \mu A$ and $-8.3 \mu A$, suggesting a gravimetrically greater SEI layer in Si/Gen2 vs Si/LiTFSI. The calculation details and estimated voltage-dependent mass density and thickness of the SEI at the pre-Li stage are presented in the Supporting Information and Fig. S3. It is possible that electrolyte-dependent reaction intermediates and SEI species with differing gravimetric properties will arise as a result of possible solvent/electrolyte redox processes that consume charge. Hence comparable currents may be observed in Si/Gen2 and Si/LiTFSI but the SEI layer mass may differ depending on the electrolyte formulations and the resulting species present in the SEI. In summary, at the pre-Li stage, electrolyte reduction and SEI formation start earlier and are more prominent in Gen2 electrolyte vs LiTFSI as evident by the larger reductive current and greater Δf at comparable potentials. The major contributor to the pre-Li SEI in Gen2 is likely due to the reductive decomposition of PF₆⁻ anion. 25

Comparison of the electrolyte-dependent post-Li vs pre-Li SEI on Si in the first electrochemical cycle.—Although SEI formation has been reported to occur in parallel with the lithiation of Si, $^{39-42}$ very little has been reported to distinguish the dynamic mass evolution of SEI from the Si lithiation process. Herein, post-lithiation SEI is defined as the SEI formation at lithiation potentials between 0.5 V and 0.001 V, referred to as the post-Li SEI (Figs. 1a-1c, yellow highlights). As lithiation of Si begins at 0.5 V, the magnitude of Δf significantly shifts to lower frequencies as represented by a steep slope of frequency decrease in contrast with the pre-Li stage (Fig. 2).

At post-Li voltages (0.5 V to 0.001 V), a larger frequency shift is seen in Gen2 as compared with LiTFSI from 0.5 V to 0.02 V with a less significant reductive current, as shown in Fig. 2b and Fig. 1b. The changes in mass density correlated to Δf at the corresponding voltage points during the *post-Li* stage are depicted in Fig. S4. Findings indicate that the Gen2 electrolyte shows greater SEIcontributed mass gain in both pre-Li and post-Li of Si as compared to LiTFSI. For instance, at 0.4 V where the onset of lithiation is started, a $-17 \mu A$ current along with $\Delta f = 133 \, Hz$ for Gen2 is shown, while a comparable current of $-19 \mu A$ is seen for LiTFSI but with a significantly less $\Delta f = 44$ Hz (Fig. 2b & Fig. S5). This trend is even more evident at a lower voltage, at 0.2 V the current and Δf for Gen2 are $-170 \mu A$ and 475 Hz as compared with a -402 μ A and a 155 Hz for LiTFSI (Fig. S5). Although LiTFSI presents a higher current, but it gives a less significant frequency shift than Gen2. Possibly suggest that the substantial loss of Li⁺ inventory in the Gen2 system contributed to the continuous SEI growth at lithiation steps, and such SEI growth is more extensive at the post-Li stage.

In summary, the above findings indicate that at lithiation voltages from 0.5 V to 0.001 V, a prominent non-faradic contribution of SEI along with a considerable SEI growth is presented in the Gen2 system as compared with the LiTFSI, and such contribution cannot be neglected. Interestingly, at a lithiation voltage of 0.001 V (deepest lithiation stage), where the formation of the fully lithiated state

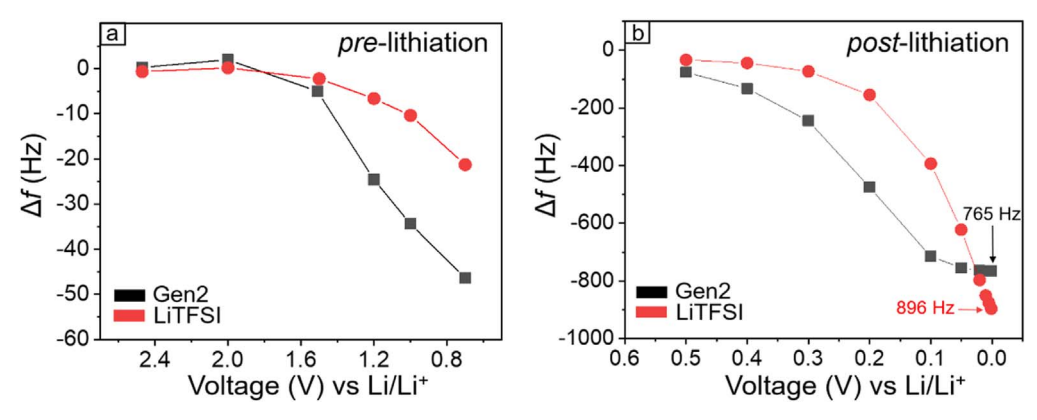


Figure 2. Voltage-dependent frequency shifts (n = 3) for Si/Gen2 and Si/LiTFSI in (a) pre-lithiation and (b) post-lithiation stages.

Li₁₅Si₄ is promoted, a maximum frequency drift of 765 Hz along with the most reductive current of $-0.8 \,\mathrm{mA}$ are seen for Gen2. However, this is not the case for LiTFSI, where the largest reducing current of −1.52 mA corresponds to a 758 Hz frequency difference observed at 0.04 V (Fig. 1b & Fig. 2b). For LiTFSI electrolyte, as the voltage continues to decrease from 0.04 V down to 0.001 V, Δf continues to drop but the maximum Δf (1100 Hz) is reached at the successive positive scan at 0.16 V which in theory is a delithiation voltage (Fig. 1c). There are two proposed potential explanations to identify the origin of this discrepancy: (1) at deep lithiation voltages, the continuous frequency drop in the LiTFSI electrolyte does not come along with a current decrease, which indicates an alloying process is possibly contributed from a continuous phase change of Si. In contrast, an equilibrium voltage of the lithium silicide formation is reached in the Gen2 system as signified by a stable frequency plateau below 100 mV (Fig. 2b); (2) the surface of the lithiated Si at deep lithiation voltages could further react with TFSI leading to a continuous formation of SEI as evidenced by an increase in frequency beyond the lowest lithiation voltage.3

FESEM and EDS analysis.—Field emission scanning electron microscopy (FESEM) micrographs and the corresponding energydispersive X-ray spectrometry (EDS) maps of Si thin film at 0.5 V and 0.001 V from the 1st electrochemical cycle in Gen2 and LiTFSI electrolytes are presented in Fig. 3. At the pre-Li stage for Si/Gen2 at 0.5 V, SEM and EDS results reveal an inhomogeneous coverage of Si (28.3% of Si signal is detected) with the formation of a fragmentary F- and P-rich SEI layer. Elemental analysis suggests major species at the Si/Gen2 interface are F (46.5%), Si (28.3%) and P (9.3%) (Fig. 3b₁-3b₄) where decomposition of PF₆⁻ appears to be the main contributor. The pre-Li SEI is likely composed of LiF rather than PF₆⁻ or PF₃ since the chemical composition of P is small compared to that of F. At the post-Li stage of Si in Gen2 at 0.001 V from the 1st electrochemical cycle, the morphology of surface layer on Si appears to be smooth and uniform without apparent island formations in contrast with the pre-Li stage (Figs. 3a-3d). Results from EDS suggest that the SEI layer, in this case, is dominated by F (40.1%), C (32.5%) and P (16.4%) where more significant

contributions come from the EC, EMC, as well as PF_6^- reduction and such findings agree with the notable frequency changes in the *post-Li* stage.

For the Si/LiTFSI, at the *pre-Li* stage at 0.5 V, significantly less electrolyte decomposition is seen in comparison with the Gen2 system, as evidenced by EDS with 8.1% of F, 6.4% of C, and 52.1% at Si/LiTFSI interface (Figs. 3f₁-3f₄). The lower presence of F and C indicates that the initial formation of the SEI in LiTFSI is less significant compared to Gen2, and this finding agrees with the minor mass density change in LiTFSI in the pre-Li stage from the EQCM-D results. Furthermore, the morphology of the pre-Li SEI in the LiTFSI electrolyte appears to be more consistent with less formation of segregated islands than in Gen2. At the post-Li stage of Si/LiTFSI at 0.001 V, a considerable increase of the fluoride (from 8.1% to 63.6%) and carbon (from 6.4% to 16.5%) signals are observed in EDS mapping as compared with the pre-Li (Figs. 3f₃, 3f₄ & 3h₂, 3 h₃). Results suggest a further TFSI reduction occurred at the deep lithiation stage which possibly leads to the formation of Li₂CNF₃, $\text{Li}_{\nu}\text{SO}_{r}$, LiF, Li_{2}S , 36,43 and this is likely triggered by the formation of a more reactive lithiated Si surface. Such a finding is in good agreement with the increased frequency shift probed by the EQCM-D as discussed in the previous sections. In addition, the morphology of the SEI surface for the post-Li stage gives a more uniform layer structure as compared with its pre-Li stage in LiTFSI, suggesting a homogeneous coverage of the F-, C- and S-rich SEI.

SEI evolution at further electrochemical cycles.—Dynamic changes of SEI at Si/Gen2 and Si/LiTFSI interfaces are further investigated at CV cycles from 1 to 6. Figure 4 presents the in situ EQCM-D measurements for the change of frequency (Δf), voltage and current for a Si thin film anode in Gen2 and LiTFSI electrolytes. Both electrolytes present a continuous baseline decrease of Δf starting at the 2nd and the 3rd CV cycles (Fig. 4c). Baseline shifts of 54 Hz, 146 Hz and 302 Hz are seen for Gen2 at the 1st, 2nd and 3rd CV cycles, while shifts of 96 Hz, 180 Hz and 282 Hz are observed for LiTFSI, at CVs 1st, 2nd and 3rd respectively. For further successive CV cycles, 4th to 6th CV cycles (Fig. 4f), baseline shifts of 430 Hz, 532 Hz and 620 Hz are seen for Gen2 at the 4th, 5th and

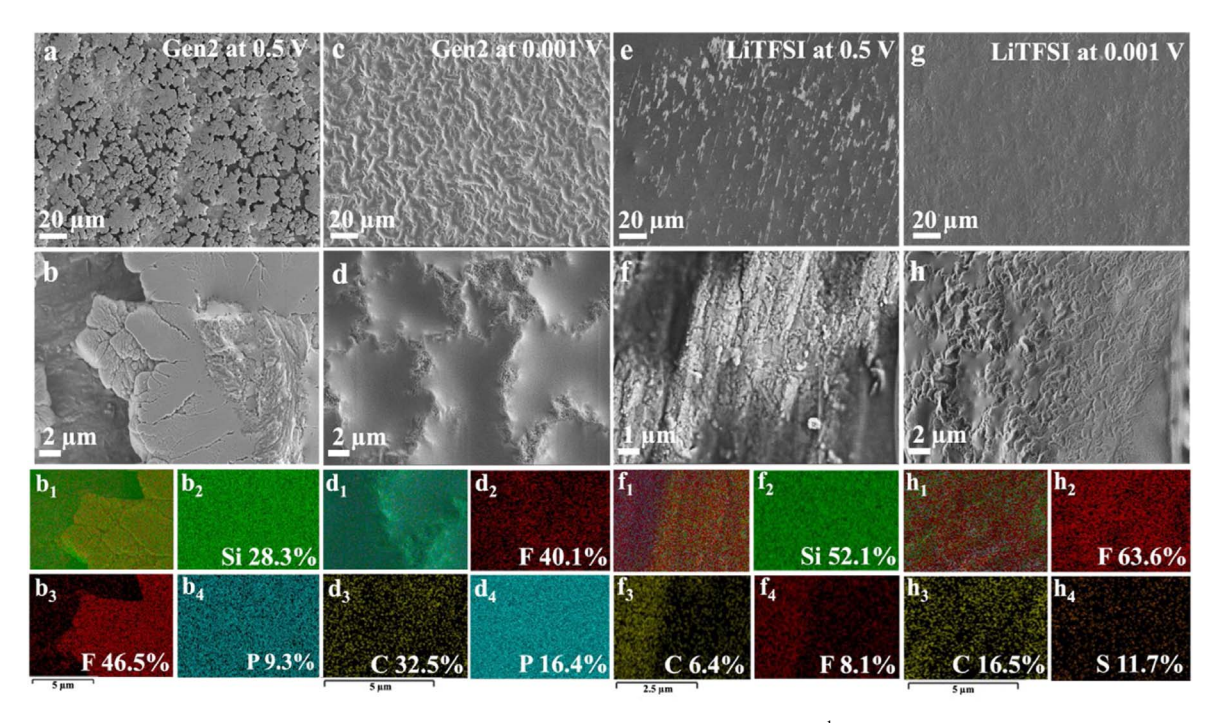


Figure 3. FESEM images and EDS mapping of Si thin film (60 nm) cycled in Swagelok cells at 1 mV s⁻¹ in Gen2 and LiTFSI. (a), (b) morphology of Si cycled in Gen2 at 0.5 V; (c), (d) morphology of Si cycled in Gen2 at 0.001 V; (e), (f) morphology of Si cycled in LiTFSI at 0.5 V; (g), (h) morphology of Si cycled in LiTFSI at 0.001 V; (b₁)–(b₄) EDS mapping of Si in Gen2 at 0.5 V; (d₁)–(d₄) EDS mapping of Si in Gen2 at 0.001 V; (f₁)–(f₄) EDS mapping of Si in LiTFSI at 0.001 V.

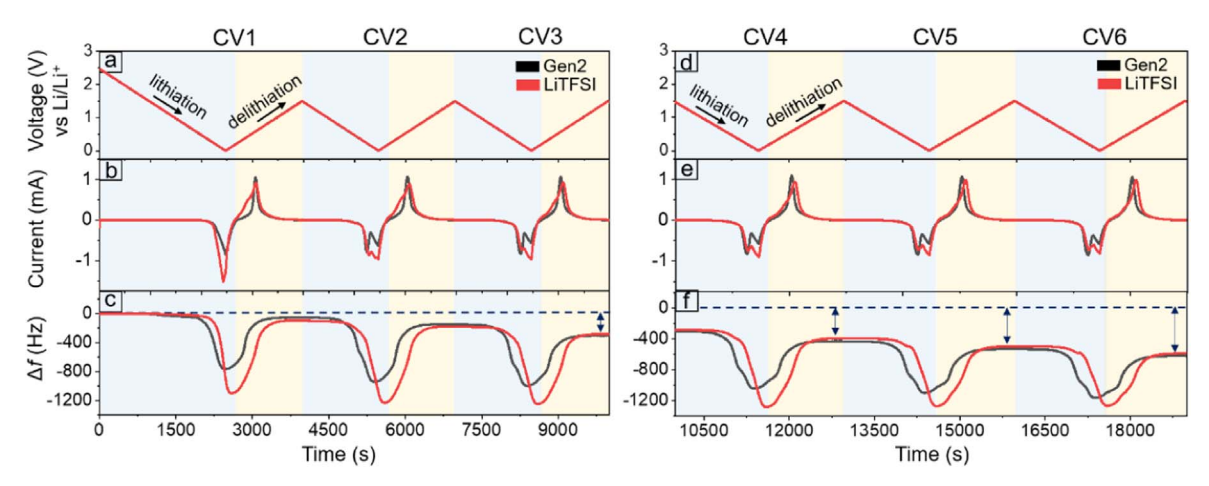


Figure 4. Frequency (Δf , n = 3), current and voltage over time for the continues (a)–(c) 1–3 CV cycles and (d)–(f) 4–6 CV cycles from OCV to 0.001 V for CV 1 and from 1.5 V to 0.001 V for CVs 2–6 at 1 mV/s for Gen2 (black curve) and LiTFSI (red curve). The blue highlight presents the lithiation process; the yellow highlight indicates the delithiation process.

6th CV cycles, while shifts of 394 Hz, 497 Hz and 590 Hz are observed for LiTFSI, respectively. Results suggest an overall thicker SEI formation happens in LiTFSI vs Gen2 at the 1st and the 2nd CV cycles, however, beyond the 3rd CV cycle, SEI in Gen2 becomes thicker than in LiTFSI as presented in Fig. S6 and Fig. S7. An increase in CE is seen for the first 2 cycles of Gen2 and the first 4 cycles for LiTFSI, as shown in Fig. S8. The calculated capacity vs CV cycle number can be found in the SI and Fig. S9. The loss of the lithium inventory is the major reason to give a lowered CE number, where both electrolytes showed the loss of Li at the initial cycles, which agrees with the shift of the frequency baseline observed.

Dissipation analysis.—Dissipation (ΔD) as a characteristic of the viscoelastic property of the deposited film is measured along the SEI formation. The increase in dissipation results from a shorter oscillatory decay of an acoustic wave that resonates from the electrode surface into the contacting liquid. ^{44,45} Results from Fig. 5 suggest both the lithiation and the delithiation processes promote the change of dissipation upon electrochemical cycling. Lithiation encourages a decrease of ΔD likely caused by the increase of viscoelastic property at Si/Gen2 and Si/LiTFSI interfaces. ⁴⁴ In contrast, delithiation promotes an increase of ΔD mainly ascribed to the hydrodynamic solid-liquid interactions suggesting non-uniform SEI evolution. ^{45,46} Upon cycling, ΔD increases indicating possible SEI growth and changes of its viscoelastic character. This

phenomenon is more significant at further cycles for both Gen2 and LiTFSI electrolytes.

For the *pre-Li* stage: an increase in dissipation is observed in Gen2 ($<5.0 \times 10^{-6}$) suggesting a hydrodynamic nature of the solidliquid interactions between the electrode and electrolyte, presented in the inset of Fig. 5b. 10 The initially formed SEI in Gen2 modifies the morphology of the electrode resulting in the increase of dissipated energy when liquid moves across the heterogeneous electrode surface. However, dissipation remains unchanged for the LiTFSI electrolyte at the *pre-Li* stage indicating an unchanged nature of its interface. For the *post-Li* stage, the change in dissipation upon Li ion insertion is observed in both Gen2 and LiTFSI electrolytes. The change in dissipation indicates a viscoelastic property of the deposited film possibly due to the soft nature of the outer organic SEI layer. 42 This finding is in agreement with the FESEM-EDS findings where a significant increase in carbon species was detected, an indication of the organic porous layer formation that is seen at the interface at post-lithiation voltages suggesting the lithiated alkoxides soft layers.

EIS analysis of the electrolyte-dependent SEI at different lithiation depths.—To further investigate the electronic properties of the SEI at the pre-Li vs the post-Li stages at Si/Gen2 and Si/LiTFSI interfaces, EIS measurements were conducted at various lithiation depths (Fig. S10) between 1.2 V and 0.001 V (fully

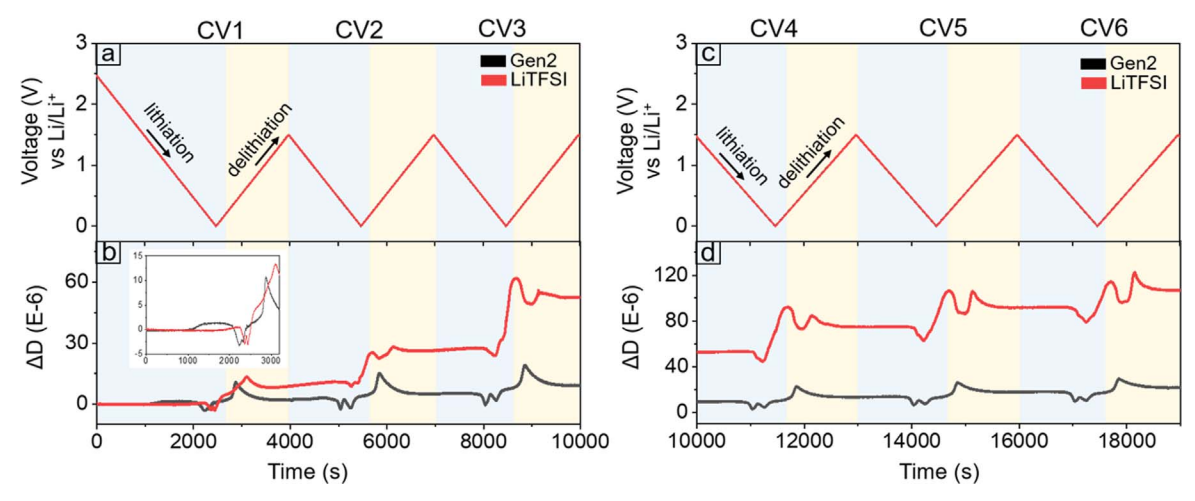


Figure 5. Voltage and dissipation changes (ΔD) over time for the continues (a)–(b) 1–3 CV cycles and (c)–(d) 4–6 CV cycles from OCV to 0.001 V for CV 1 and from 1.5 V to 0.001 V for CVs 2–6 at 1 mV/s for Si/Gen2 (black curve) and Si/LiTFSI (red curve). The inset in panel b displays the magnification of the lithiation and delithiation region of the first electrochemical cycle.

discharged state). The electronic elements of R_{ct} , R_{SEI} , Q_{ct} , Q_{SEI} , R_{s} and W represent the charge transfer resistance, the SEI resistance, charge transfer capacitance, SEI capacitance, electrolyte resistance and the Warburg component, respectively. These parameters were obtained by fitting the experimental EIS data to the equivalent circuit model with the AfterMath software. The experimental and fitted Nyquist plots are presented in Fig. 6, and fitted data are tabulated in Table S1

For the pre-Li voltages, EIS at two representative potentials of 1.2 V and 0.5 V is selected. A depressed semicircle at the high-tomiddle frequency region is seen at 1.2 V with $R_{ct} = 82~\Omega$ and 450 Ω for Gen2 and LiTFSI, respectively. The initial high Rct in LiTFSI indicates the absorption step that is coupled with the early SEI formation stage, which involves a sluggish de-solvation process associated with a higher energy penalty, in agreement with the electrochemical signal in Fig. 1.50 Such absorption step comes along with a capacitance of $Q_{ct} = 72.7 \ \mu s/\Omega$ in LiTFSI indicating an evident charge accumulation at the interface. At pre-Li voltage of 0.5 V, EIS presents a less deformed semicircle as compared to 1.2 V, such a change of geometry indicates the emergence of a new interfacial process. To identify such surface evolution, two RC circuits are applied to better describe the new interfacial development. A significant change of R_{ct} in LiTFSI electrolyte is observed, with R_{ct} decreasing from 450 Ω (at 1.2 V) to 250 Ω (at 0.5 V) presented in Fig. 6e. This suggests an enhanced interfacial charge transfer kinetics due to the LiF formation at the interface evidenced by the EDS findings (F content increases from 8% to 63%). R_{ct} remains unchanged for Gen2 electrolyte at 1.2 V to 0.5 V (Fig. 6b). R_{SEI} in LiTFSI is slightly larger than in Gen2 at 0.5 V likely due to the initial surface absorption process (15.5 Ω vs 5.9 Ω).

For the *post-Li* stage, EIS at three representative potentials 0.01 V, 0.005 V and 0.001 V are chosen. A new interfacial process emerges for the Gen2 electrolyte at the *post-Li* stage with a prominent increase in R_{SEI} from 5.9 Ω to \sim 30 Ω , suggesting a SEI growth triggered by the increased reactivity of the lithiated Si surface. S1.52 While a less depressed semicircle is seen in LiTFSI electrolyte with further decrease of R_{ct} (270 Ω at 0.5 V to 227 Ω at

0.01 V) as compared with the *pre-Li* stage, followed by subsequent stabilization. The improved R_{ct} is seen in LiTFSI and is possibly ascribed to the formation of a more kinetically facile network of Si structure with the increase of Li ion content in Si lattice $(Si \rightarrow Li_xSi)$.⁵³ The interface forming over time could benefit charge transfer kinetics by reducing the energy required for stripping off the Li⁺ ion's solvation shell.⁵⁴ Additionally, the Warburg element is modeled in series with R_{ct} representing the impedance associated with the lithium ion diffusion to the bulk Si, represented by the straight line in the low-frequency range (10–0.05 Hz) as shown in Figs. 6a, 6d. At the post-*Li* stage, the increase in the phase angle (ϕ) vs the lithiation depth is seen for both Gen2 and LiTFSI (Table S1), for instance, an increase of ϕ from 45° at 0.5 V to 63° at 0.001 V is seen in Gen2 with a similar trend in LiTFSI from 42° to 50° at comparable potentials. The increase of the phase angle to the values above 45° demonstrates improved interfacial kinetics.⁵⁵

Overall, in comparison to the Gen2 vs the LiTFSI electrolytes, $R_{\rm SEI}$ in Gen2 is higher while $R_{\rm ct}$ in LiTFSI is higher. Results suggest that an earlier formed fluorinated SEI in Si/Gen2 benefits the charge transfer kinetics, while an initial inert SEI is detected in Si/LiTFSI and is converted to a facile charge transfer kinetics at the interface upon lithiation. The $R_{\rm SEI}$ slightly increases in Gen2 as lithiation progresses due to additional interfacial development.

FTIR analysis.—The FTIR spectra were collected for Si thin film cycled with Gen2 and LiTFSI electrolytes to 0.5 (*pre-Li*) and 0.001 V (*post-Li*) and are presented in Fig. 7. The FTIR spectra of Si/Gen2 in Figs. 7a, 7b presents the adsorption bands characteristic of typical decomposition products of carbonate solvents such as ROCO₂Li, Li₂CO₃ and R–CO₂–Li as evidenced by the existence of the C–O, C–O–O and C–H stretching vibrations in the spectral range of 1850 – 1000 cm⁻¹. ^{56,57} Further reactions of Li₂CO₃ with HF may promote the formation of LiF and H₂O as evident by the appearance of broad bands at 3600–3000 cm⁻¹ from ν H–O and a peak at 1633 cm⁻¹ assigned to δ H–O–H. ⁵⁸ Additionally, peaks at 1250, 840 and 662 cm⁻¹ may be assigned to the stretching modes of P=O, P–F and Li–F generated from LiPF₆ decompositions. ^{57,59}

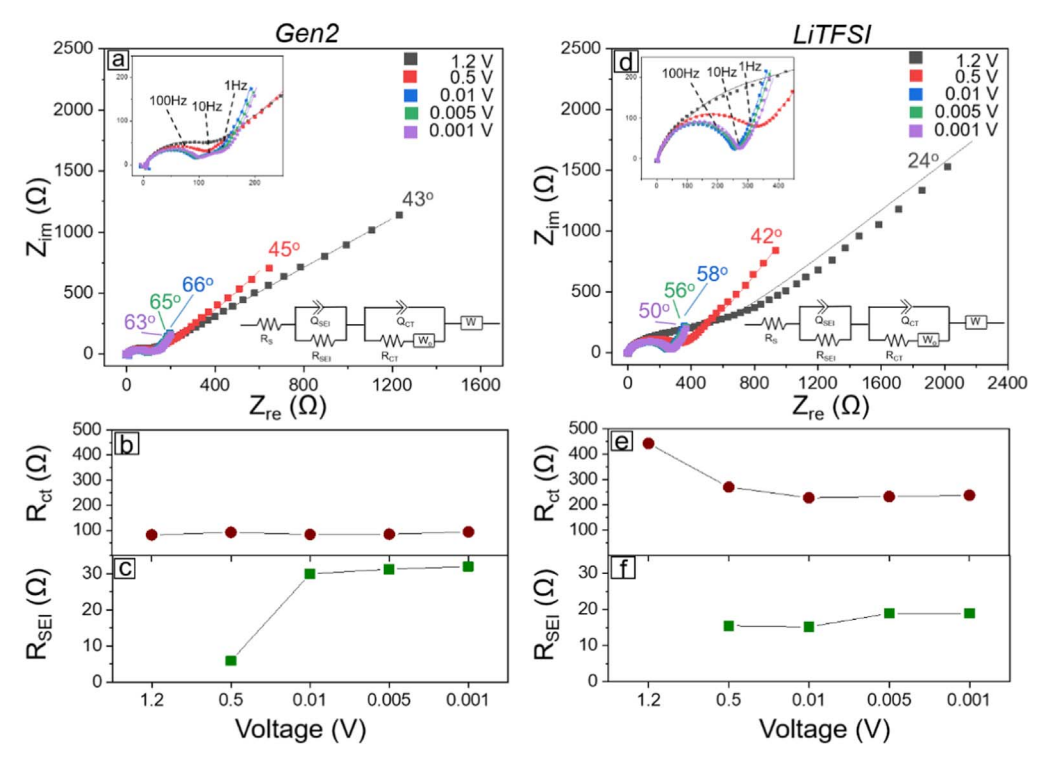


Figure 6. (a) Nyquist spectra at different lithiation depths for Si/Gen2 and its corresponding (b) R_{ct} and (c) R_{SEI} values; (d) Nyquist spectra at different lithiation depths for Si/LiTFSI with corresponding (e) R_{ct} and (f) R_{SEI} values; EIS is collected in a two-electrode Swagelok cell (Si thin film vs Li) with the frequency range from 0.05 Hz to 1 M Hz. Insets in panels a and d display the magnified high-frequency region.

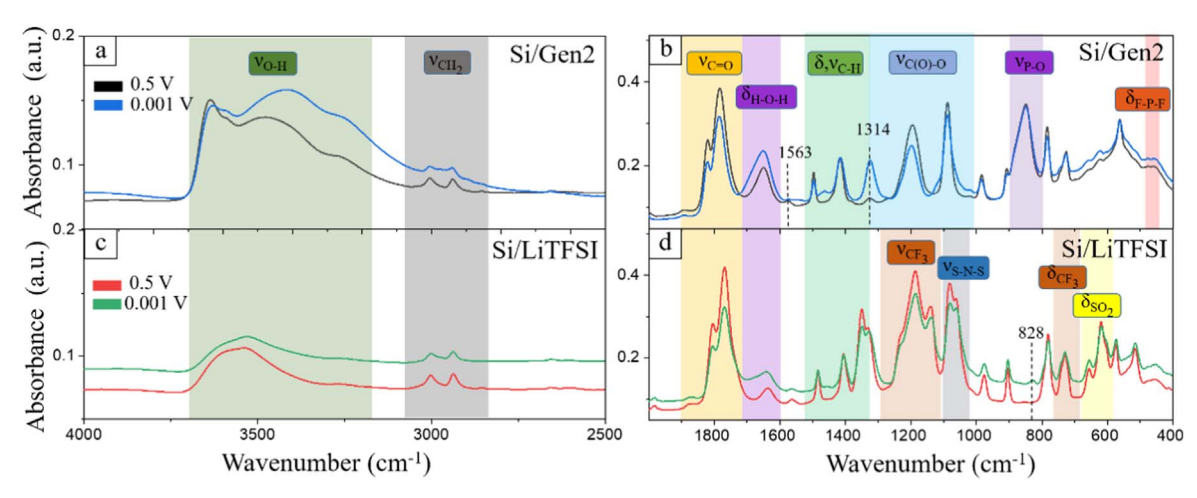


Figure 7. FTIR spectra of the electrochemically cycled Si thin film in (a)–(b) Gen2; (c)–(d) LiTFSI. Peak positions marked with black dashed lines are unique to each spectrum.

The most significant changes between the *pre-Li* and *post-Li* conditions in Si/Gen2 are evident at 0.5 V at 1563 cm⁻¹ which indicates the formation of Li propionate, the product of EMC and EC decomposition. But this feature is not apparent at 0.001 V. Worth to mention that a small feature at 1314 cm⁻¹ is observed at 0.5 V and increases in intensity at 0.001 V which is a characteristic of C-H of lithium ethylene dicarbonate (LiEDC) formed via the reduction of EC and reaction with Li at the interface. Go.61 Therefore, the FTIR analysis indicates that the SEI layer for Si/Gen2 is primarily composed of organic compounds with functionalities of alkyl, carboxylate metal salt, and Li–F and P–F containing inorganic species consistent with the FESEM/EDX results. While the disappearance of Li propionate and increase in the concentration of LiEDC is observed in Si/Gen2 at *post-Li* voltage down to 0.001 V due to the reaction of EC with exposed lithiated silicon.

On the other hand, the FTIR spectra of Si/LiTFSI in Figs. 7c, 7d presents a feature at 828 cm⁻¹ that is likely ascribed to the stretching mode of Si–F detected in the *post-Li* stage at 0.001 V. But this feature is not seen in *pre-Li* stage at 0.5 V, possibly suggesting further TFSI reduction takes place on lithiated silicon surface which is consistent with the FESEM/EDX showing an increase in F, C, and S signals from TFSI reduction at the deep lithiation (Figs. 3h1–3h4). 62,63 The FTIR spectra also show the vibration modes ascribed to the products of carbonate solvent decomposition similar to those observed in Si/Gen2. Additional distinct peaks emerge in the spectral range of 1500 – 500 cm⁻¹ assigned to the various C–F, S–N–S and S–O stretching modes from the products of TFSI anion decomposition. 62,64 These findings indicate the SEI layer in the *post-Li* stage in Si/LiTFSI is dominated by the products of TFSI decomposition rather than carbonate solvent decomposition.

Conclusions

In this work, the in situ SEI evolution is probed to reveal its electrochemical, gravimetric, electronic, and chemical properties on a thin film Si anode in Gen2 and LiTFSI electrolytes by the in situ EQCM-D measurements with EIS and FESEM/EDS analysis. The electrolyte-dependent in situ SEI formation and evolution are evaluated and contrasted in two stages of lithiation, *pre-Li* vs *post-Li* stages. In the *pre-Li* stage, results reveal an earlier SEI formation and a more prominent SEI growth in Gen2 vs the LiTFSI electrolytes. For the *pre-Li* SEI: a Si/Gen2 interface reveals an inhomogeneous morphology with a F- and P-rich SEI, in contrast to a homogeneous and less segregated surface morphology in Si/LiTFSI interface with a low detected concentration of F and C species. In the *post-Li* stage, at the deepest lithiation stage (1 mV vs Li), the greatest frequency shift is accompanied by the largest reductive current in Si/Gen2, while for Si/LiTFSI the highest mass

gain is not seen until the successive delithiation occurred. The oxidation stability of TFSI possibly prevents the generation of fluorinated species in Si/LiTFSI at the pre-Li stage leading to higher $R_{\rm ct}$ in contrast to Si/Gen2 where a LiF-rich layer is formed that facilitates the charge transfer kinetics. Findings imply a possible continuous surface evolution of Si/LiTFSI interface with active TFSI decompositions in post-Li, which comes along with a significant increase of the F, C and S chemical components and improved interfacial kinetics. This work suggests different SEI evolution pathways in Gen2 vs LiTFSI where a thicker and gravimetrically greater contribution to SEI for Gen2 at the pre-Li stage is evident.

Acknowledgments

This work is financially supported by the National Science Foundation (NSF), the NSF CAREER grant (no. 2047753). The Office of Energy Efficiency and Renewable Energy of the Vehicle Technologies Program at the U.S. Department of Energy is gratefully acknowledged for the Si Consortium Project. Acquisition of the advanced FESEM is acknowledged from the MRI grant of the National Science Foundation (Grant No. 1919919). Proposal Development Grant from the University of Massachusetts Boston is acknowledged. The authors would like to thank Steve Shepard and his support from the cleanroom of the Boston College Integrated Sciences. The authors thank Dr. Baris Key and Dr. John Vaughey at Argonne National Lab for their contributions.

ORCID

References

- Y. X. Zhang, B. R. Wu, G. Mu, C. W. Ma, D. B. Mu, and F. Wu, *J. Energy Chem.*, 64, 615 (2022).
- M. N. Obrovac, L. Christensen, D. B. Le, and J. R. Dahnb, J. Electrochem. Soc., 154, A849 (2007).
- 3. C. Y. Wang, C. P. Yang, and Z. J. Zheng, Adv. Sci., 9, 2105213 (2022).
- 4. D. L. Ma, Z. Y. Cao, and A. M. Hu, Nano-Micro Lett., 6, 347 (2014).
- 5. C. M. Park, J. H. Kim, H. Kim, and H. J. Sohn, Chem. Soc. Rev., 39, 3115 (2010).
- B. Key, R. Bhattacharyya, M. Morcrette, V. Seznec, J. M. Tarascon, and C. P. Grey, J. Am. Chem. Soc., 131, 9239 (2009).
- D. Uxa, B. Jerliu, E. Huger, L. Dorrer, M. Horisberger, J. Stahn, and H. Schmidt, J. Phys. Chem. C, 123, 22027 (2019).
- 8. M. T. McDowell, S. W. Lee, W. D. Nix, and Y. Cui, Adv. Mater., 25, 4966 (2013).
- 9. M. N. Obrovac and L. Christensen, *Electrochem. Solid-State Lett.*, 7, A93 (2004).
- 10. J. Y. Kwon, J. H. Ryu, and S. M. Oh, *Electrochim. Acta*, 55, 8051 (2010).
- T. Z. Hou, G. Yang, N. N. Rajput, J. Self, S. W. Park, J. Nanda, and K. A. Persson, *Nano Energy*, 64, 1038812 (2019).
- C. C. Nguyen, T. Yoon, D. M. Seo, P. Guduru, and B. L. Lucht, ACS Appl. Mater. Inter., 8, 12211 (2016).

- C. C. Nguyen, D. M. Seo, K. W. D. K. Chandrasiri, and B. L. Lucht, *Langmuir*, 33, 9254 (2017).
- I. A. Shkrob, J. F. Wishart, and D. P. Abraham, J. Phys. Chem. C, 119, 14954 (2015).
- 15. K. Xu. Chem. Rev., 104, 4303 (2004).
- M. Y. Nie, D. Chalasani, D. P. Abraham, Y. J. Chen, A. Bose, and B. L. Lucht, J. Phys. Chem. C, 117, 1257 (2013).
- L. Z. Lv, Y. Wang, W. B. Huang, Y. Y. Wang, G. B. Zhu, and H. H. Zheng, *Electrochim. Acta*, 413, 140159 (2022).
- A. V. Plakhotnyk, L. Ernst, and R. Schmutzler, J. Fluorine Chem., 126, 27 (2005).
- B. Philippe, R. Dedryvere, M. Gorgoi, H. Rensmo, D. Gonbeau, and K. Edstrom, Chem. Mater., 25, 394 (2013).
- D. E. Arreaga-Salas, A. K. Sra, K. Roodenko, Y. J. Chabal, and C. L. Hinkle, J. Phys. Chem. C, 116, 9072 (2012).
- J. M. M. de la Hoz, F. A. Soto, and P. B. Balbuena, J. Phys. Chem. C, 119, 7060 (2015).
- V. Chakrapani, F. Rusli, M. A. Filler, and P. A. Kohl, J. Power Sources, 205, 433
 (2012)
- Q. Zhou, P. D. Boyle, L. Malpezzi, A. Mele, J. H. Shin, S. Passerini, and W. A. Henderson, *Chem. Mater.*, 23, 4331 (2011).
- M. Y. Nie, D. P. Abraham, Y. J. Chen, A. Bose, and B. L. Lucht, *J. Phys. Chem. C*, 117, 13403 (2013).
- 25. P. Verma, P. Maire, and P. Novak, *Electrochim. Acta*, 55, 6332 (2010).
- 26. E. Markevich et al., J. Electrochem. Soc., 160, A1824 (2013).
- 27. H. Y. Mou, W. Xiao, C. Miao, R. Li, and L. M. Yu, Front. Chem., 8, 141 (2020).
- 28. M. N. Vila et al., ACS Appl. Mater. Inter., 14, 20404 (2022).
- G. M. Veith, M. Doucet, R. L. Sacci, B. Vacaliuc, J. K. Baldwin, and J. F. Browning, Sci Rep., 7, 6326 (2017).
- M. T. Ong, O. Verners, E. W. Draeger, A. C. T. van Duin, V. Lordi, and J. E. Pask, J. Phys. Chem. B, 119, 1535 (2015).
- D. M. Seo, S. Reininger, M. Kutcher, K. Redmond, W. B. Euler, and B. L. Lucht, J. Phys. Chem. C, 119, 14038 (2015).
- T. Kawaguchi, K. Shimada, T. Ichitsubo, S. Yagi, and E. Matsubara, J. Power Sources, 271, 431 (2014).
- D. M. Seo, O. Borodin, S. D. Han, P. D. Boyle, and W. A. Henderson, *I. Electrochem. Soc.* 159, A1489 (2012)
- J. Electrochem. Soc., 159, A1489 (2012).
 D. Aurbach, O. Chusid, I. Weissman, and P. Dan, Electrochim. Acta, 41, 747 (1996).
- 35. C. C. Nguyen, S. W. Woo, and S. W. Song, J. Phys. Chem. C, 116, 14764 (2012).
- V. Sharova, A. Moretti, T. Diemant, A. Varzi, R. J. Behm, and S. Passerini, J. Power Sources, 375, 43 (2018).
- Z. Z. Yang, M. C. Dixon, R. A. Erck, and L. Trahey, ACS Appl. Mater. Inter., 7, 26585 (2015).
- G. R. V. Zhuang, K. Xu, H. Yang, T. R. Jow, and P. N. Ross, J. Phys. Chem. B, 109, 17567 (2005).

- S. Benning, C. G. Chen, R. A. Eichel, P. H. L. Notten, and F. Hausen, ACS Appl. Energy Mater., 2, 6761 (2019).
- F. A. Soto, J. M. M. de la Hoz, J. M. Seminario, and P. B. Balbuena, Curr. Opin. Chem. Eng., 13, 179 (2016).
- C. T. Cao, H. G. Steinrck, B. Shyam, and M. F. Toney, *Adv. Mater. Interfaces*, 4, 1700771 (2017).
- 42. C. T. Cao, H. G. Steinruck, B. Shyam, K. H. Stone, and M. F. Toney, *Nano Lett.*,
- 7394 (2016).
 G. G. Eshetu, T. Diemant, S. Grugeon, R. J. Behm, S. Laruelle, M. Armand, and S. Passerini, ACS Appl. Mater. Inter., 8, 16087 (2016).
- 44. N. Shpigel, M. D. Levi, and D. Aurbach, *Energy Storage Mater.*, 21, 399 (2019).
- N. Shpigel, M. D. Levi, S. Sigalov, L. Daikhin, and D. Aurbach, Accounts Chem. Res., 51, 69 (2018).
- A. A. Hubaud, Z. Z. Yang, D. J. Schroeder, F. Dogan, L. Trahey, and J. T. Vaughey, J. Power Sources, 282, 639 (2015).
- 47. S. K. Heiskanen, J. Kim, and B. L. Lucht, Joule, 3, 2322 (2019).
- B. T. Young, D. R. Heskett, C. C. Nguyen, M. Y. Nie, J. C. Woicik, and B. L. Lucht, ACS Appl. Mater. Inter., 7, 20004 (2015).
- B. S. Parimalam, A. D. MacIntosh, R. Kadam, and B. L. Lucht, *J. Phys. Chem. C*, 121, 22733 (2017).
- J. T. Hu, H. D. Guo, Y. W. Li, H. B. Wang, Z. Q. Wang, W. Y. Huang, L. Y. Yang, H. B. Chen, Y. Lin, and F. Pan, *Nano Energy*, 89, 106413 (2021).
- B. H. Han, C. Liao, F. Dogan, S. E. Trask, S. H. Lapidus, J. T. Vaughey, and B. Key, ACS Appl. Mater. Inter., 11, 29780 (2019).
- Y. Xu, K. Wood, J. Coyle, C. Engtrakul, G. Teeter, C. Stoldt, A. Burrell, and A. Zakutayev, *J. Phys. Chem. C*, 123, 13219 (2019).
- J. M. Su, J. Y. Zhao, L. Y. Li, C. C. Zhang, C. G. Chen, T. Huang, and A. S. Yu, ACS Appl. Mater. Inter., 9, 17807 (2017).
- G. Hernandez, A. J. Naylor, Y. C. Chien, D. Brandell, J. Mindemark, and K. Edstrom, ACS Sustain. Chem. Eng., 8, 10041 (2020).
- A. J. Bard and L. R. Faulkner, Electrochemical Methods: Fundamentals and Applications (New York, Wiley) (2000).
- W. J. Tang, W. J. Peng, G. C. Yan, H. J. Guo, X. H. Li, and Y. Zhou, *Ionics*, 23, 3281 (2017).
- 57. R. T. Pekarek et al., J. Mater. Chem. A, 8, 7897 (2020).
- 58. K. Xu, Chem. Rev., 104, 4303 (2004).
- 59. S. W. Song and S. W. Baek, Electrochem. Solid-State Lett., 12, A23 (2009).
- F. F. Shi, P. N. Ross, G. A. Somorjai, and K. Komvopoulos, J. Phys. Chem. C, 121, 14476 (2017).
- D. E. Arreaga-Salas, A. K. Sra, K. Roodenko, Y. J. Chabal, and C. L. Hinkle, J. Phys. Chem. C, 116, 9072 (2012).
- A. Lahiri, N. Borisenko, A. Borodin, M. Olschewski, and F. Endres, *Phys. Chem. Chem. Phys.*, 18, 5630 (2016).
- D. J. Michalak, S. R. Amy, D. Aureau, M. Dai, A. Esteve, and Y. J. Chabal, *Nat. Mater.*, 9, 266 (2010).
- 64. C. C. Nguyen and S. W. Song, *Electrochem. Commun.*, 12, 1593 (2010).